Agricultural and Forest Meteorology 259 (2018) 184–195

Contents lists available at ScienceDirect

Agricultural and Forest Meteorology

journal homepage: www.elsevier.com/locate/agrformet

Changes in photosynthesis and soil moisture drive the seasonal soil respiration-temperature hysteresis relationship

Quan Zhang[a,b,*], Richard P. Phillips[c], Stefano Manzoni[d,e], Russell L. Scott[f], A. Christopher Oishi[g], Adrien Finzi[h], Edoardo Daly[i], Rodrigo Vargas[j], Kimberly A. Novick[b]

[a] State Key Laboratory of Water Resources and Hydropower Engineering Science, Wuhan University, Wuhan, China
[b] School of Public and Environmental Affairs, Indiana University, Bloomington, IN, USA
[c] Department of Biology, Indiana University, Bloomington, IN, USA
[d] Department of Physical Geography, Stockholm University, Stockholm, Sweden
[e] Bolin Center for Climate Research, Stockholm University, Stockholm, Sweden
[f] Southwest Watershed Research Center, USDA-ARS, Tucson, AZ, USA
[g] USDA Forest Service, Southern Research Station, Coweeta Hydrologic Laboratory, Otto, NC, USA
[h] Department of Biology, Boston University, Boston, MA, USA
[i] Department of Civil Engineering, Monash University, Clayton, Victoria, Australia
[j] Department of Plant and Soil Sciences, University of Delaware, Newark, DE, USA

ARTICLE INFO

Keywords:
CO_2 efflux
FLUXNET
Q_{10} model
Time lag

ABSTRACT

In nearly all large-scale terrestrial ecosystem models, soil respiration is represented as a function of soil temperature. However, the relationship between soil respiration and soil temperature is highly variable across sites and there is often a pronounced hysteresis in the soil respiration-temperature relationship over the course of the growing season. This phenomenon indicates the importance of biophysical factors beyond just temperature in controlling soil respiration. To identify the potential mechanisms of the seasonal soil respiration-temperature hysteresis, we developed a set of numerical models to demonstrate how photosynthesis, soil moisture, and soil temperature, alone and in combination, affect the hysteresis relationship. Then, we used a variant of the model informed by observations of soil respiration, soil temperature, photosynthesis, and soil moisture from multiple mesic and semi-arid ecosystems to quantify the frequency of hysteresis and identify its potential controls. We show that the hysteresis can result from the seasonal cycle of photosynthesis (which supplies carbon to rhizosphere respiration), and soil moisture (which limits heterotrophic respiration when too low or too high). Using field observations of soil respiration, we found evidence of seasonal hysteresis in 9 out of 15 site-years across 8 diverse biomes. Specifically, clockwise hysteresis occurred when photosynthesis preceded seasonal soil temperature and counterclockwise hysteresis occurred when photosynthesis lagged soil temperature. We found that across all sites, much of the respiration-temperature lag was explained by the decoupling of photosynthesis and temperature, highlighting the importance of recently assimilated carbon to soil respiration. An analysis of observations from 129 FLUXNET sites revealed that time lags between gross primary productivity (a proxy for canopy photosynthesis) and soil temperature were common phenomena, which would tend to drive counterclockwise hysteresis at low-latitude sites and clockwise hysteresis at high-latitude sites. Collectively, our results show that incorporating photosynthesis and soil moisture in the standard exponential soil respiration-temperature model (i.e., Q_{10} model) improves the explanatory power of models at local scales.

1. Introduction

Soil respiration (R_s; i.e., the sum of autotrophic and heterotrophic respiration in the soil) is the largest terrestrial carbon (C) source to the atmosphere. Consequently, small changes in the magnitude of R_s can produce considerable fluctuations in atmospheric CO_2 concentration (Raich and Schlesinger, 1992) and impact global climate. Soil temperature (T_s) is typically the dominant factor controlling the rate of R_s, often explaining most of its variability (Bond-Lamberty and Thomson, 2010a; Davidson et al., 1998; Lloyd and Taylor, 1994), with numerous studies demonstrating that R_s responds exponentially to T_s in ecosystems where water is not limiting (Luo et al., 2001; Zhang et al., 2013).

* Corresponding author at: State Key Laboratory of Water Resources and Hydropower Engineering Science, Wuhan University, Wuhan, 430072, China.
E-mail addresses: quan.zhang@whu.edu.cn, quazhang@indiana.edu (Q. Zhang).

https://doi.org/10.1016/j.agrformet.2018.05.005
Received 9 June 2017; Received in revised form 24 March 2018; Accepted 7 May 2018

Table 1
Observed seasonal soil respiration-temperature hysteresis in previous studies.

Method[a]	Temperature depth (cm)[b]	Hysteresis direction[c]	Suggested factors[d]	Ecosystem type or species[e]	Sources
GC	0[f]	2	substrate supply	mixed forest	Crill (1991)
DCS	5	1	NA	grassland	Knapp et al. (1998)
DCS	NA	2	NA	Sphagnum moss	Goulden et al. (1998)
DCS	5	2	NA	conifer boreal forest	Morén and Lindroth (2000)
DCS	5	2	temperature profile, root respiration	Pseudotsuga menziesii	Drewitt et al. (2002)
DCS	15	NA	NA	Ponderosa pine	Irvine and Law (2002)
NA	NA	1[g]	substrate depletion	NA	Kirschbaum (2004)
DCS	7.5	1	NA	grassland	Verburg et al. (2005)
DCS	15	1, 8	seasonal temperature, soil moisture pattern, and phenology	grassland	Harper et al. (2005)
DCS	5	1[h]	NA	Pseudotsuga menziesii	Jassal et al. (2005)
DCS	2	2	decomposable litter	deciduous forest	Curiel Yuste et al. (2005)
NA	NA	1	substrate depletion	NA	Kirschbaum (2006)
DCS	2	1	soil moisture, fine root production	Populus tremuloides	Gaumont-Guay et al. (2006)
GM222	8	1	root respiration	mixed temperate forest	Vargas and Allen (2008)
DCS	2	2, 8	vegetation type, soil structure	mixed forest	Phillips et al. (2010)
DCS	0, 5, 10	1	root phenology and litterfall	mixed forest	Oe et al. (2011)
DCS	5	1	heterotrophic respiration	mixed temperate forest	Kominami et al. (2012)
DCS	10	2	soil microbial activity, fresh litter	Pinus tabulaeformis plantation	Jia et al. (2013)

a- GMM222: type of probes for CO_2 concentration measurements (soil respiration is calculated based on gas gradient method); GC: gas chromatograph method (air was collected and CO_2 was analyzed by chromatograph); DCS: dynamic closed system containing an Infra-Red Gas Analyzer (IRGA) and a chamber, including the commonly used commercial LI-8100, LI-8100A, LI-6400 systems and other self-made systems; NA: no field measurements were conducted, and numerical methods were used to generate soil respiration.
b- NA: no clear information for depth of temperature measurement, or results are based on model runs.
c- 1: clockwise, 2: counterclockwise, 8: "figure-8"-shaped pattern, NA: no direction was suggested, nor was there sufficient information to derive the direction.
d- All studies suggested factors by speculation.
e- NA: that soil respiration was obtained from numerical methods.
f- Air temperature.
g- Fall has lower respiration rate than spring; the direction is therefore supposed to be clockwise.
h- Greater sensitivity in the latter part of the year; the direction is therefore supposed to be clockwise.

However, in many ecosystems, cycles of R_s are often out of phase with cycles of T_s, leading to hysteresis in the R_s-T_s relationship at both diurnal (see Zhang et al., 2015) and seasonal timescales (see Table 1).

Such hysteresis has been observed most frequently at the diurnal scale, and there is a rich body of literature explaining the mechanisms that control this pattern. First, the dynamics of soil heat flow can cause soil temperature in different soil layers to peak at different times of the day (Phillips et al., 2011; Zhang et al., 2015). Second, the dynamics of gas transport in the soil is affected by soil moisture and soil structure, which determine how efficiently respired CO_2 is transported to the surface where it is measured (Zhang et al., 2015). Finally, the dynamics of photosynthesis and carbon allocation can also affect diurnal hysteresis by regulating the availability of substrate to soil microbes and the rhizosphere (Abramoff and Finzi, 2015; Oikawa et al., 2014; Stoy et al., 2007; Vargas and Allen 2008; Zhang et al., 2015). While reports of hysteresis occurring at seasonal scales have also been widely reported (Table 1), the drivers of these seasonal patterns are poorly understood and no consensus has emerged to explain them.

One challenge to uncovering a single explanation for the hysteresis relationship is that the nature of the hysteresis may differ. In nearly 40% of the previous studies in Table 1, increases in R_s lag increases in T_s, generating a counterclockwise hysteresis (i.e., R_s at a given temperature is lower during the early growing season than during the late growing season). Such a dynamic could occur when photosynthesis is in phase with T_s, but there is a long lag in the delivery of substrate to the roots or microbes (Crill, 1991; Jia et al., 2013, see Table 1) either through allocation processes or through litterfall (Curiel Yuste et al., 2005). In contrast, in ~50% of the studies in Table 1, increases in R_s precede increases in T_s, resulting in a clockwise hysteresis (i.e., R_s at a given temperature is greater during the early growing season than during the late growing season). This sort of pattern could be explained by progressive substrate depletion over the course of the growing season (Kirschbaum, 2006), by greater root productivity early in the growing season (Oe et al., 2011) or by soil moisture (θ) limitation to soil respiration late in the season (Gaumont-Guay et al., 2006). In addition to these two patterns (i.e., counterclockwise and clockwise), a "figure-8" pattern at the diurnal scale (Zhang et al., 2015) can also characterize seasonal dynamics (e.g., Harper et al., 2005; Phillips et al., 2010, Table 1). This pattern may result from different sensitivities of autotrophic and heterotrophic respiration to their drivers (Song et al., 2015). For example, although both autotrophic and heterotrophic respiration respond positively to T_s (Zhang et al., 2013), a higher temperature sensitivity is commonly assumed for autotrophic respiration (Boone et al., 1998; Savage et al., 2013; Zhang et al., 2013), whereas heterotrophic respiration may be more sensitive to soil moisture (Moyano et al., 2013). Thus, a critical challenge is not merely to understand why hysteresis occurs, but to identify the frequency of environmental conditions conducive to seasonal clockwise, counterclockwise or figure-8 hysteresis.

The primary objective of this work is to present a generalizable framework to elucidate the key mechanisms responsible for generating the various hysteresis patterns at the seasonal timescale. We test the hypotheses that the compound effects of photosynthesis and θ together with T_s are major drivers of the seasonal hysteresis, and the time lag between gross primary productivity (GPP) and T_s is an important factor driving the temporal decoupling of R_s and T_s. We expect that counterclockwise hysteresis will be most common at sites where GPP lags T_s, clockwise hysteresis will be most common at sites where GPP precedes T_s, and the figure-8 pattern will be most common at sites where the dynamics of θ and GPP are out of phase, but both are important in controlling soil respiration. We test these hypotheses by merging field observations with numerical models of R_s that accommodates a variety of mechanisms which may be responsible for seasonal R_s-T_s hysteresis.

2. Method and theory

We present two sets of mathematical approaches to disentangle the drivers of the seasonal hysteresis. First, we use a conceptual numerical model to illustrate how different time lags among T_s, GPP and θ can alter the shape of the seasonal R_s-T_s hysteresis. Second, we use observations of R_s, T_s, GPP, and θ from a range of biomes to parameterize quasi-empirical variants of the numerical model for R_s, which are then used to interpret the observed patterns of hysteresis at these sites. Here we assume that T_s, GPP, and θ impact R_s independently; in the discussion, we address some limitations of this assumption and the potential for interactions among these drivers.

2.1. Developing a simple model with conceptual mathematical representation of the hysteresis

As the first step in our analysis, we develop a simple mathematical model for soil respiration that accommodates the drivers (e.g., temperature, GPP, and θ) which we hypothesized to be primarily responsible for seasonal hysteresis. The results emerging from the analysis of this theoretical model will inform our understanding of dynamics observed in field observations.

In most models, R_s is simulated based on its exponential relationship with temperature (T, which represents a generic temperature of either soil or air temperature). Here, we also Great! considered GPP (used as a proxy of canopy photosynthesis rate) and θ as key factors driving R_s at the local scale. For each driver (T, GPP, and θ), a response function of R_s (χ) was specified together with seasonal cycles of the driver. To focus on the role of seasonal phase shift among the drivers, all values of the drivers were normalized to fall between 0 and 1. Likewise, the response functions associated with each driver were also normalized so that they ranged from a minimum value, when the driver has no effect, to 1, when the effect of the driver reaches it maximum. For the response function of T (Eq. (1.1)), we adopted a Q_{10} model (Lloyd and Taylor, 1994):

$$\chi_T = e^{b(T-T_{max})} \tag{1.1}$$

where T_{max} is the maximum seasonal temperature, and b is a temperature sensitivity coefficient.

The response function of θ (Eq. (1.2)) was assumed to be quadratic, thus accounting for the suppression of soil respiration at both high and low θ (Suseela et al., 2012; Zhang et al., 2013):

$$\chi_\theta = 1-\left(\frac{\theta}{\theta_0}-1\right)^2, \tag{1.2}$$

where θ_0 is the saturation level at maximum respiration (near soil field capacity) so that $\frac{\theta}{\theta_0}$ is a non-dimensional value reflecting effects of θ. The response function of GPP (Eq. 1.3) was assumed to be linear (Tang et al., 2005; Zhang et al., 2013):

$$\chi_{GPP} = \chi_{GPP,0} + (1-\chi_{GPP,0})GPP \tag{1.3}$$

where the parameter $\chi_{GPP,0}$, if positive, allows soil respiration to occur even in the absence of plant carbon uptake due to heterotrophic activity. See Fig. S1 in the supplementary information (SI) for an illustration of these response functions.

To describe the seasonal cycles of each driver, we used generic non-negative sine functions:

$$y = \frac{1}{2}(1 + \sin(ft + \phi_y)) \tag{2}$$

where y is either T, GPP or θ ; f is 2π $year^{-1}$ so that the period of all drivers is 1 year, t is time within the one-year interval, and ϕ_y is the phase angle shift with respect to a reference phase. Here, the phase of the T series was set to $\phi_T = 0$, such that the phase shifts of GPP and θ were defined relative to the phase of T. A positive phase shift indicates that GPP and θ peak before T.

The compound environmental effects on R_s were then modeled by different combinations of Eqs. (1.1)–(1.3) as:

$$\chi(T,GPP) = \chi_T(\phi_T)\chi_{GPP}(\phi_{GPP}) \tag{3.1}$$

$$\chi(T,\theta) = \chi_T(\phi_T)\chi_\theta(\phi_\theta) \tag{3.2}$$

$$\chi(T, GPP,\theta) = \chi_T(\phi_T)\chi_{GPP}(\phi_{GPP})\chi_\theta(\phi_\theta) \tag{3.3}$$

where Eq. (3.1) combines the effects of GPP and T on R_s, Eq. (3.2) combines θ and T, and Eq. (3.3) combines all the three factors.

To explore how GPP, θ and their combinations regulate the temperature response of R_s, the response functions (i.e., Eqs. (3.1)–(3.3)) were plotted as a function of T under various ϕ_{GPP} and ϕ_θ values. The area enveloped by the loop can be used to quantify the hysteresis magnitude as proposed by Zhang et al. (2014). The phase shifts of ϕ_{GPP} and ϕ_θ with respect to T were set at π/6, 0 and – π/3 for Eqs. (3.1) and (3.2); the phase shifts were selected as typical cases to show how positive, zero and negative shifts regulate the shape and direction of the hysteresis between R_s and T. As Eq. (3.3) includes the effect of three variables, we considered scenarios where ϕ_θ was set to π/6, 0 and – π/3, and for each considered ϕ_{GPP} = π/6 and ϕ_{GPP} =– π/3. By normalizing the drivers, we limit the focus of this analysis to the effects associated with phase shifts alone.

2.2. Diagnosing and modeling hysteresis in field measurements

We adapt the model structure described above into a more commonly-used Q_{10} form that can be readily parameterized using field observations, facilitating an assessment of how well the hypothesized drivers of seasonal hysteresis can be captured by the more commonly-used Q_{10} approach. In this exercise, the drivers were not normalized to one. However, the shapes of the functional relationships between R_s and each driver are similar to those presented in Eqs. (1.1)–(1.3). In the Q_{10} model here, R_s is described as a function of T_s (Lloyld and Taylor, 1994) as

$$R_s = R_{ref}\, e^{bT_s} \tag{4}$$

where R_{ref} is the basal respiration when T_s = 0 °C, and b is the temperature sensitivity coefficient, linked to Q_{10} via $Q_{10} = e^{10b}$.

Similar to Eq. (1.3), R_s is assumed to be a linear function of canopy photosynthesis (Tang et al., 2005; Zhang et al., 2013) as

$$R_s = a_g GPP + b_g \tag{5}$$

To simultaneously consider both temperature and canopy photosynthesis, we assume that basal respiration correlates with canopy photosynthesis (Sampson et al., 2007). This requires linking R_{ref} in Eq. (4) to GPP in a way that is also consistent with the linear dependence assumed in Eq. (5). To this aim, the linear dependence in Eq. (5) was normalized to obtain a non-dimensional factor that varies between 0 and 1 and rescales respiration as a function of GPP; this factor was then multiplied by a new reference respiration value and R_s was modeled as:

$$R_s = R_{ref,GPP}\frac{\frac{GPP}{GPP_{max}} + n}{1 + n}e^{bT_s} \tag{6}$$

where $R_{ref,GPP}$ is the new reference rate, the parameter n defines the role of GPP as a driver of R_s (n = 0 → strongest effect of GPP), and GPP_{max} is the maximum measured value of GPP. When GPP = GPP_{max}, the second term on the right-hand side of Eq. (6) equals one, indicating that GPP is not limiting soil respiration. In contrast, as GPP decreases the second term also decreases to the minimum value of $n/(1+n)$, which represents the contribution of heterotrophic respiration to the reference respiration, in absence of contributions from recent photosynthates. The parameter *n* thus reflects the fact that freshly assimilated carbohydrates are not the only substrate available to microbes to respire and heterotrophic respiration is also associated with the

decomposition of soil organic matter. In Eq. (6), R_s increases with increasing n following a saturating curve to capture limiting factors that bound soil respiration to an upper limit independent of GPP ($R_s \rightarrow R_{ref,GPP}e^{bT_s}$ when $n \gg 1$).

To account for the soil moisture effects in the Q_{10} approach, we follow the commonly used quadratic dependence of R_s on θ to account for the suppression of R_s at both high and low θ conditions (Suseela et al., 2012; Zhang et al., 2013). Accordingly,

$$R_s = R_{ref,\theta}[1-c(\theta-\theta_{opt})^2]e^{bT_s} \quad (7)$$

where $R_{ref,\theta}$ is the reference rate when soil moisture is included as a predictor of respiration, θ_{opt} is the optimal soil moisture at which soil respiration reaches its maximum value, and c is a shape parameter reflecting the importance of soil moisture as a driver of R_s ($c = 0 \rightarrow$ least effect of θ). As in Eq. (6), the second term on the right-hand side of Eq. (7) is non-dimensional and varies between 0 and 1 (when $\theta = \theta_{opt}$).

In parallel with the simple models assuming that either canopy photosynthesis and temperature (Eq. (6)) or soil moisture and temperature (Eq. (7)) regulate basal respiration, we constructed a full model including all three factors (T_s, GPP and θ):

$$R_s = R_{ref,GPP,\theta}\frac{\frac{GPP}{GPP_{max}}+n}{1+n}[1-c(\theta-\theta_{opt})^2]e^{bT_s} \quad (8)$$

where $R_{ref,GPP,\theta}$ is a new reference rate. As in the previous equations, all the rate modifiers are non-dimensional coefficients that vary between 0 and 1. The parameter values were obtained from a calibration against field measurements by minimizing the sum of square errors between measurements and the modeled values.

2.3. Statistical criteria for model quality

The goodness of fit was evaluated using the coefficient of determination (R^2) and root mean square error (RMSE), and an F-test was applied to assess the significance level. Because the aforementioned numerical models have different input and parameters, we applied the Akaike's Information Criterion (AIC, Akaike, 1987) as a criteria for model comparison. Low values of AIC are associated with better model performance. The AIC value of different models is calculated as:

$$AIC = N\log(\hat{\sigma}^2) + 2k \quad (9)$$

where N is the number of the data sample, $\hat{\sigma}^2$ is the residual variance used to estimate the maximum likelihood function, k is the number of model parameters.

In general, AIC performs poorly in cases with relatively little data (low N value) and numerous parameters (high k value); therefore we used a corrected AIC (AIC_c) (Burnham and Anderson, 2002) as:

$$AIC_c = AIC + \frac{2k(k+1)}{N-k-1} \quad (10)$$

2.4. Site description and data collection

To characterize the hysteresis and parameterize the model of Eqs. (4)–(8), we used observed time series from eight sites within the AmeriFlux network that span a gradient of climate and vegetation conditions (Table 2). In all sites, R_s was monitored continuously using dynamic closed chambers at intervals ranging from 0.5 to 2 h. Additionally, we took advantage of girdled experiments that were conducted at two sites (US-MMS and US-SRM, see below for more details). Because girdling restricts the movements of C in the phloem from reaching the roots, measurements of R_s in girdled vs. control plots allowed us to assess the extent to which the R_s-T_s hysteresis was driven by autotrophic vs. heterotrophic controls.

Three of our study sites were located in the Duke Forest in central North Carolina: the Duke Forest Hardwood (AmeriFlux Site, US-Dk2), the Duke Forest Loblolly Pine (AmeriFlux Site, US-Dk3), and a nearby "Old Pine" site (not yet part of AmeriFlux, referred to as "Duke-OP" hereafter). At each site, R_s was measured using an Automated Carbon Efflux System (ACES, USDA Forest Service, US Patent 6,692,970). Each system consists of 15 soil chambers, which alternated between two locations for 3–4 day periods. Thus, there are effectively up to 30 individual sampling locations, and we obtained a continuous R_s series by aggregating all individual measurements. Soil temperature at 10 cm depth was measured with thermistors (334-NTC102-RC, Xicon Passive Components, Mansfield, TX), and soil moisture averaged over the upper 30 cm depth was measured with time domain reflectometry sensors (CS-615, Campbell Scientific, Logan, UT, USA). More details regarding R_s collections can be found in Oishi et al. (2013). Data used for US-Dk2 are from 2003 and 2004, US-Dk3 are from 2006, and Duke-OP are from 2004; these years satisfy the requirement of having measurements covering at least an entire year.

The Morgan Monroe State Forest (AmeriFlux Site, US-MMS) is located in south-central Indiana, where conditions are cooler and drier than the Duke Forest. At US-MMS, eight soil collars were set in a single area, dominated by several species of Quercus (oak). In mid-July 2011, a girdling experiment was established (Brzostek et al., 2015), whereby all trees inside four 15 m × 15 m plots were girdled, thereby reducing belowground carbohydrate supply from photosynthesis. Four nearby non-girdled plots, which consisted of the same tree species as the girdled plots, were used as controls. We have effectively 4 control plots and 4 girdled plots. One chamber was placed in each plot, and R_s was measured in each plot once per hour with a ~450 s measurement interval. The automated lid on each chamber was closed prior to measurements, and a tube head was used to pump air to the gas analyzer station, which was programmed to analyze air temperature, relative humidity, CO_2 mole fraction, and atmospheric pressure every second. The 451 s measurement interval includes 90 s during which the program switched between chambers. Soil effluxes were calculated using a method similar to the calculations with an LI-8100 (LiCOR, Lincoln, NE, USA). Model fits with a coefficient of determination (R^2) less than 0.9 were rejected from analyses. Adjacent to each soil collar, a thermocouple was inserted 5 cm into the ground for temperature measurement. A time domain reflectometry sensor (CS-616, Campbell Scientific) was inserted 30 cm into the ground, approximately in the center of all 8 plots for continuous soil moisture measurement. The R_s measurements operated through 2012.

The Harvard Forest (AmeriFlux Site, US-Ha1) is located in central Massachusetts and has cooler conditions than US-MMS. At Harvard Forest, R_s measurements were collected separately from two different experiments. The first experiment (hereafter named US-Ha1-E1) was conducted in 2003 and had 6 replicate chambers (Savage et al., 2008); soil temperature and soil moisture were monitored concurrently using a 10 cm probe and a 15 cm TDR, respectively, both inserted vertically into the ground. The second experiment (hereafter named US-Ha1-E2) was conducted from 2003 through 2006 along a moisture gradient from the edge of a wetland to upland by using 8 chambers (Phillips et al., 2010); soil temperature at 2 cm depth was collected, but soil moisture was not. In both experiments, soil CO_2 concentration was continuously measured, and again, the method similar to LI-8100 (LiCOR) calculations was used to calculate R_s. For more methodological details, see Savage et al. (2008) (for US-Ha1-E1) and Phillips et al. (2010) (for US-Ha1-E2).

The Santa Rita Mesquite Savanna (AmeriFlux site, US-SRM) and Walnut Gulch Kendall Grasslands (AmeriFlux site, US-Wkg) are both semi-arid ecosystems that experience higher temperatures and lower amounts of precipitation relative to all other sites. At US-SRM, automated chambers (LI-8100, LiCOR) were used to measure R_s under intact mesquite tree canopies with 3 replicates (control plot), under mesquite tree canopies that were girdled with 3 replicates (girdled plot), and in the inter-canopy space occupied by bunchgrasses with 2 replicates (open plot) in 2015. The chambers were set over soil collars inserted 8

Table 2
Characteristics of the selected sites. MAT (°C) and MAP (mm) are mean annual temperature and mean annual precipitation, respectively.

Site ID	Location	MAT (°C)	MAP (mm)	Ecosystem type	Reference
US-Dk2	35°58 N, 79°08 W	14.36	1170	Deciduous Broadleaf Forest	Novick et al. (2009)
US-Dk3	35°58 N, 79°08 W	14.36	1170	Evergreen Needleleaf Forest	Novick et al. (2009)
Duke-OP	35°58 N, 79°08 W	14.36	1170	Evergreen Needleleaf Forest	Novick et al. (2009)
US-MMS	39°19' N, 86°25' W	10.8	1094	Deciduous Broadleaf Forest	Schmid et al. (2000)
US-Ha1(E1)	42°54' N, 72°17' W	6.62	1071	Deciduous Broadleaf Forest	Savage et al. (2008)
US-Ha1(E2)	42°54' N, 72°17' W	6.62	1071	Deciduous Broadleaf Forest	Phillips et al. (2010)
US-SRM	31°49' N, 110°52' W	19	380	Savanna	Scott et al. (2015)
US-Wkg	31°44' N, 109°56' W	17	350	Grassland	Scott et al. (2015)

cm into the ground, and the system was programmed to monitor air temperature, relative humidity, CO_2 mole fraction, and atmospheric pressure every second during 90 s measurement intervals every 2 h. R_s was obtained using the LI-8100 software, and chamber runs where the model R^2 was less than 0.9 were rejected from analyses. Close to each chamber, one soil thermistor and soil moisture probe were installed at 5 cm depth. At US-Wkg, the same type of soil chambers used in US-SRM were deployed at four locations in 2016. Soil temperature and moisture were monitored with the same protocol as US-SRM.

In all of the study sites, NEE was partitioned into GPP and ecosystem respiration (ER) by fitting nighttime NEE to a function of soil or air temperature. This function was used to estimate daytime respiration, and GPP was then calculated as –NEE + ER. At US-MMS, a single exponential function of surface soil temperature was fitted using nighttime NEE measurements for the entire year, following the approach of Schmid et al. (2000) and Sulman et al. (2016). At Harvard Forest, nighttime NEE was fitted to air temperature within a fixed ~10-day window (Munger and Wofsy, 1999, Harvard Forest Data Archive: HF004). The same approach was used for US-SRM and US-Wkg but with a 5-day moving window that did not overlap a rain event (see Scott et al., 2015). At Duke Forest, NEE was partitioned using the Van Gorsel et al. (2009) approach as described in Novick et al. (2015). This approach still relies on using nocturnal data to parameterize a temperature-dependent model for ER; however, the data are subjected to a stricter set of filters designed to minimize contributions from periods of likely horizontal and vertical advection. We use these site-specific GPP products to preserve consistency between results presented here and previous work from these sites.

2.5. Field data processing and analysis

Time series of R_s data often contain spikes and errors due to gas analyzer failure and rain events. Therefore, all measurements were filtered to exclude these data. To account for spatial variability, R_s measurements were averaged by treatment types (i.e., 'control', 'girdled' and 'open' if any) at each site. Because this study is focused on hysteresis at the seasonal timescale, the original measurement series (with a resolution from half hour to ~2 h) were averaged into two-week intervals to reduce the noise associated with high-frequency measurements. The two-week interval is also consistent with the averaging period adopted in many previous studies listed in Table 1. To test that a two-week window was not too large (possibly hiding dynamics that might affect the relationship between variables at the seasonal scale), time lags were also estimated using one-day and one-week windows. The results from this analysis are similar to those obtained with a two-week window (Fig. S2 in the SI), which are presented throughout the main text. All observations, including T_s, GPP and θ, were also aggregated into two-week intervals accordingly.

Our hypotheses state that phase shifts between key driving and response variables are primarily responsible for generating the observed hysteresis. To quantify the time lags (or offsets) between R_s and T_s, as well as the time lag between GPP and T_s, a cross correlation analysis was conducted. Two data series X and Y were thus related as:

$$Y(t) = aX(t-h) + b \quad (10)$$

where t is time and h is the lag (both t and h are defined by a unit increment corresponding to 2 weeks), and a and b are regression parameters. To evaluate the time lag, X was shifted both forward (positive h) and backward (negative h) by an interval of h (h = 1, 2, 3, …); Y was then linearly regressed with the newly generated shifted time series (i.e., X(t–h)), and finally the best-fit regression (i.e., maximum R^2) was used to identify the time lag.

2.6. GPP and soil temperature time lag within FLUXNET2015 dataset

As a final step in the analysis, we determined the potential for lags between GPP and T_s to drive the seasonal hysteresis across a wide range of biomes by extending the cross-correlation analysis to data from 129 sites in the FLUXNET2015 Tier1 dataset (http://fluxnet.fluxdata.org/data/fluxnet2015-dataset/). We selected the T_s measured closest to the surface and used the GPP product based on the nighttime partitioning approach by Reichstein et al. (2005). We only used original measurements or gap-filled data of good quality (gap filling flag = 0 represents original measurement, while gap filling flag = 1 or 2 represent gap filling with high or medium quality). The GPP-T_s lag was then evaluated at all sites of the FLUXNET2015 Tier1 dataset by using the aforementioned methods (Eq. (10)), and using a time step of one week.

3. Results

3.1. Simulating soil respiration-temperature hysteresis using conceptual models

Combining GPP and T in the R_s models successfully generated hysteresis in the relationship between R_s and T (Fig. 1a). Specifically, a clockwise hysteresis appeared when the annual peak of T lagged GPP (red curve in Fig. 1a), while a counterclockwise hysteresis appeared when the annual peak of T preceded GPP (black curve in Fig. 1a). The extent of the hysteresis increased as a function of the absolute phase angle difference and shrunk to zero when GPP and T were in phase (blue curve in Fig. 1a). When effects of θ and T were incorporated into the model, a figure-8 loop emerged (Fig. 1b), with the direction of the loop dependent on the value of the phase angle shift of θ. Combining GPP, θ and T with various phase angle shift combinations generated more diverse patterns in the hysteresis relationships (Fig. 1c and d)

3.2. Hysteresis in field measurements and numerical models

Nearly all hysteresis patterns that have been reported in previous studies were represented in the field data considered here (Fig. S3). We present three typical patterns in Fig. 2, i.e., the clockwise direction in US-Dk2 in 2003 (Fig. 2a), the counterclockwise direction of the control plot in US-SRM (Fig. 2b) and the figure-8 pattern in US-Wkg (Fig. 2c) (see Table 3 and Fig. S3 in the SI for all sites). Although seasonal hysteresis effects were strong, T_s still explained much of the seasonal variation of R_s in the mesic sites of US-Dk2, US-Dk3, Duke-OP, US-MMS, US-Ha1-E1 and US-Ha1-E2 (R^2 range 0.64–0.94, see Table 4).

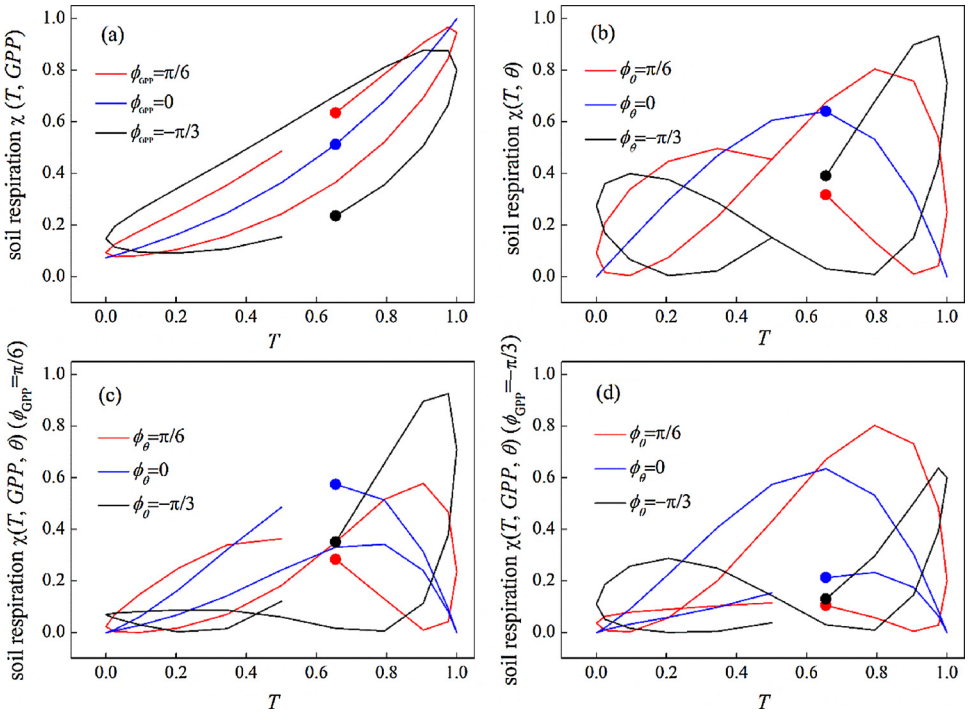

Fig. 1. Dependence of normalized soil respiration (χ in Eqs. (3.1), (3.2) and (3.3)) on temperature (T) under various scenarios by combining (a) temperature and gross primary productivity (GPP) with phase angle shifts of π/6, 0 and −π/3 (positive values indicate GPP precedes T, and negative values indicate GPP lags T), (b) temperature and soil moisture (θ) with phase angle shifts of π/6, 0 and −π/3 (positive values indicate θ precedes T, and negative values indicate θ lags T), (c) temperature, GPP with phase angle shift of π/6 and soil moisture with phase angle shifts of π/6, 0 and −π/3, (d) temperature, GPP with phase angle shift of −π/3 and soil moisture with phase angle shifts of π/6, 0 and −π/3. Solid dots denote the start of the seasonal cycle when t = 0 in Eq. (2) (For interpretation of the references to color in this figure legend, the reader is referred to the web version of this article).

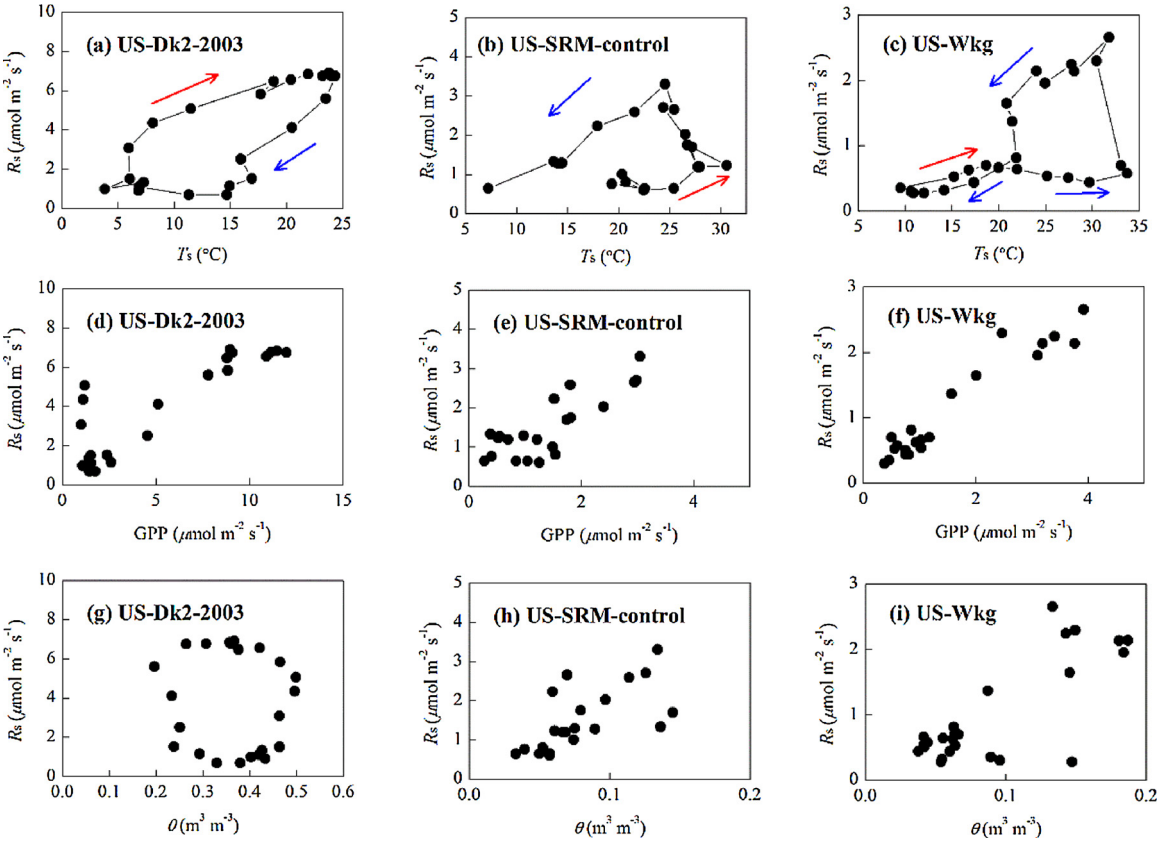

Fig. 2. Measured hysteresis patterns of soil respiration (R_s) in response to soil temperature (T_s) at the three representative sites (a) US-Dk2 of 2003, (b) US-SRM control plot and (c) US-Wkg; the arrows indicate the progression of a year cycle, with the red and blue arrows indicating the first and second half of the cycle, respectively; (d–f) the dependence of R_s on gross primary productivity (GPP, used as a proxy for canopy photosynthesis supporting root and rhizosphere respiration) at the three sites; (g–i) the relationship between R_s and soil moisture (θ) at the three sites (For interpretation of the references to color in this figure legend, the reader is referred to the web version of this article).

Table 3
Summary of the hysteresis direction in the field measurements.

Counterclockwise	Clockwise	Figure-8 pattern
Duke-OP	US-Dk2-2003	US-Dk2-2004
US-SRM-control	US-Dk3	US-MMS-control
US-SRM-girdled		US-MMS-girdled
US-SRM-open		US-Wkg
US-Ha1-E2-2003		US-Ha1-E1
US-Ha1-E2-2004		US-Ha1-E2-2005
US-Ha1-E2-2006		

However, at the semi-arid sites (US-SRM and US-Wkg), T_s poorly explained the variation in seasonal R_s across treatments (R^2 range 0.06–0.40, see Table 4). In addition to T_s, GPP also correlated well with total soil respiration (comprised of root and heterotrophic respiration) across sites (Fig. 2d–f as examples, see Fig. S4 in the SI for all sites), and can explain 52–90% of seasonal variations in R_s (Table 4). Soil moisture had no discernible effects on R_s across the mesic sites (Fig. 2g as an example for US-Dk2, see Fig. S5 for other mesic sites). At the semi-arid sites of US-SRM and US-Wkg, a positive linear function of θ explained 20–43% of the variation in R_s (data not shown, but see Fig. S5g-i and j in the SI).

Across all sites, the seasonal time lag between GPP and T_s was strongly correlated with the lag between R_s and T_s (Fig. 3); a possible interpretation of this correlation is that respiration of recently assimilated carbon has a strong impact on seasonal respiration rates. After incorporating GPP and the parameter *n* in Eq. (6), which implicitly reflects the contribution of photosynthate to root respiration in the Q_{10} model, the hysteresis patterns at most sites were reproduced more accurately than by a simple temperature-dependent model (Fig. 4a–c for representative examples, and Fig. S6 for all sites), with improvements in R^2 (Table 4) and RMSE (compare Table S2 and S1). Model improvement was also reflected by the lower AIC_c of Eq. (6) compared with that of Eq. (4) at most sites, indicating that adding the variable GPP and parameter n is statistically justifiable. Hence, Eq. (6), which incorporates GPP, was able to reproduce the R_s-T_s hysteresis by capturing the phase angle of R_s, because the time lag was close to 0 between modeled and measured R_s series (data not shown). However, incorporating GPP did not capture the hysteresis at US-Ha1-E2 (Fig. S6i-l).

Similarly, after incorporating θ in the Q_{10}-based temperature response function (Eq. (7)), the model improvement was pronounced in most sites, as reflected by the increased R^2, as well as lowered AIC_c (Table 4) and RMSE (Table S3). Including θ effects in the model further improved agreement between the simulations and the observations at several sites, including the clockwise hysteresis at US-Dk2 of 2003 (Fig. 4d), counterclockwise behavior at US-SRM-control (Fig. 4e), and the figure-8 pattern at the US-Wkg (Fig. 4f). See Fig. S7 for all sites.

The full model, which incorporated both GPP and θ constraints into the Q_{10}-based temperature response function (Eq. (8)) when data w ere available, was able to reproduce all the observed hysteresis dynamics (Fig. 4g–i as examples, see Fig. S8 for all sites) with relatively higher R^2 (Table 4) and lower RMSE than the simpler models (Table S4). However, the model performance was not necessarily improved when comparing AIC_c with the scenarios considering T_s alone, considering GPP alone, combining T_s and GPP, and combining T_s and θ (Table 4).

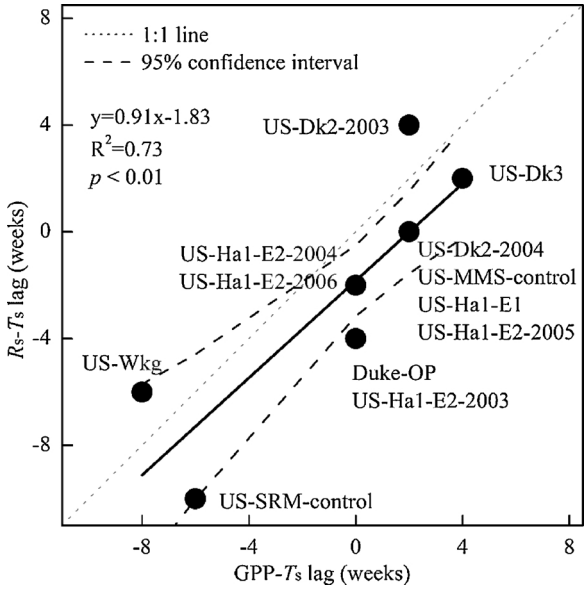

Fig. 3. Cross-site synthesis of the relationship between soil respiration-soil temperature (R_s-T_s) time lag and the GPP-soil temperature (GPP-T_s) lag. Note that negative values of GPP-T_s lag indicate that the annual peak of GPP lags soil temperature, and the negative values of R_s-T_s time lag indicate that soil respiration lags soil temperature.

Table 4
Performance of soil respiration predictive equations based on soil temperature (Eq. (4)), GPP (Eq. (5)), soil temperature and GPP (Eq. (6)), soil temperature and soil moisture (Eq. (7)), soil temperature, GPP and soil moisture (Eq. (8)). Here, the performance was evaluated by means of the coefficient of determination (R^2) or the adjusted R^2 (adj. R^2) and the corrected Akaike's Information Criterion scores (AIC_c). AIC_C scores should be compared only across models for a single site. The root mean square error (RMSE), the significance level of the fitting (p) and the fitted parameters can be found in Table S1–S4 in supplementary information.

Site	Eq. (4)		Eq. (5)		Eq. (6)		Eq. (7)		Eq. (8)	
	R^2	AICc	R^2	AICc	adj.R^2	AICc	adj.R^2	AICc	adj.R^2	AICc
US-Dk2-2003	0.64	22.00	0.76	12.63	0.73	14.78	0.71	20.03	0.75	20.09
US-Dk2-2004	0.85	−11.41	0.74	2.16	0.84	−9.94	0.83	−6.34	0.85	−5.18
US-Dk3	0.92	−15.92	0.89	−9.71	0.94	−26.31	0.93	−18.62	0.95	−26.48
Duke-OP	0.79	−7.39	0.86	−15.63	0.84	−14.18	0.86	−14.24	0.90	−17.96
US-MMS-control	0.68	−28.92	0.87	−49.93	0.87	−50.01	0.76	−31.64	0.91	−49.03
US-MMS-girdled	0.86	−18.94					0.87	−18.20		
US-SRM-control	0.06	−7.02	0.67	−28.75	0.61	−26.01	0.46	−15.94	0.75	−29.11
US-SRM-girdled	0.31	−25.21					0.71	−40.54		
US-SRM-open	0.40	−42.62					0.75	−58.06		
US-Wkg	0.25	−16.18	0.93	−64.57	0.92	−62.98	0.89	−61.16	0.95	−68.47
US-Ha1-E1	0.94	−15.04	0.52	14.61	0.95	−18.08	0.93	−7.69	0.95	−9.43
US-Ha1-E2-2003	0.82	−15.78	0.74	−9.82	0.77	−12.02				
US-Ha1-E2-2004	0.90	−20.25	0.80	−6.67	0.89	−18.12				
US-Ha1-E2-2005	0.90	−8.63	0.90	−8.39	0.89	−7.15				
US-Ha1-E2-2006	0.80	−12.4	0.67	−2.68	0.75	−8.37				

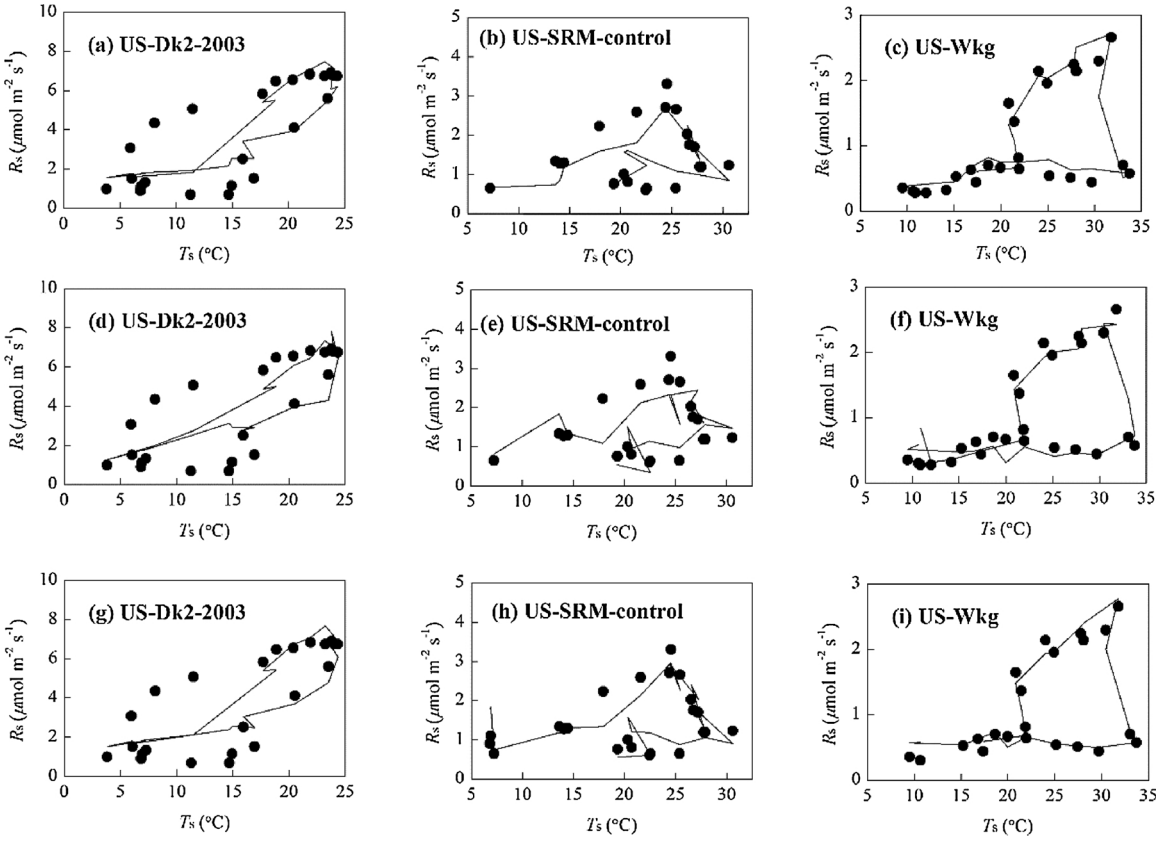

Fig. 4. Hysteresis loops reproduced by combining Q_{10} model and photosynthesis (GPP) effect (Eq. (6)) (a–c), Q_{10} model and soil moisture (Eq. (7)) (d–f), and Q_{10} model and the two factors of photosynthesis and soil moisture (Eq. (8)) (g–i). Lines represent model simulations and symbols are observations.

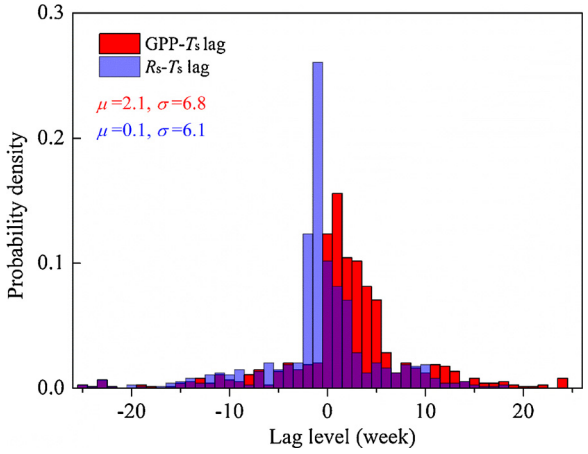

Fig. 5. Probability density functions of the time lag between GPP and soil temperature (GPP-T_s lag, red bars), and soil respiration and soil temperature (R_s-T_s lag, blue bars) predicted by the relationship from Fig. 3 for 737 site-years (129 sites) in the FLUXNET2015 Tier1 dataset (For interpretation of the references to color in this figure legend, the reader is referred to the web version of this article).

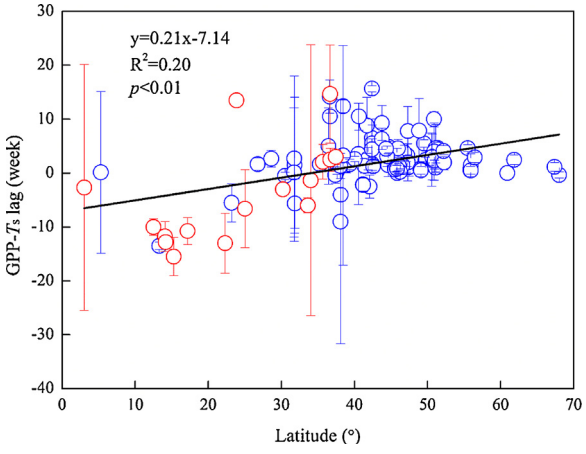

Fig. 6. Relationship between latitude and time lags of GPP and soil temperature (GPP-T_s lag) evaluated for the FLUXNET2015 dataset; red points refer to the southern hemisphere, and blue points refer to the northern hemisphere (For interpretation of the references to color in this figure legend, the reader is referred to the web version of this article).

3.3. Extending the scope of the analysis to FLUXNET sites

By leveraging the FLUXNET2015 Tier1 dataset, we found that the GPP-T_s lag spans a wide range from −25 to 25 weeks, with a mean (μ) and standard deviation (σ) of 2.1 and 6.8 weeks, respectively (Fig. 5). The GPP-T_s lag also showed strong inter-annual variation at the site level (see Table S5 for details). Spatially, the GPP-T_s lag varies with latitude (Fig. 6); specifically, it ranges from negative values at low latitudes to positive values with increasing latitude. Additionally, the GPP-T_s lag depends on vegetation type (Fig. 7), with savannas and closed shrublands on the two ends of GPP-T_s lag spectrum. In savannas, GPP is more likely to lag T_s with a mean GPP-T_s lag of −8.8 weeks, whereas in closed shrublands, GPP is more likely to precede T_s with a mean GPP-T_s lag of 6.6 weeks. The GPP-T_s lags for other vegetation types fall within the aforementioned range. Using the relationship in Fig. 3, GPP-T_s lag predicts a mean of 0.1 week for the R_s-T_s lag for the FLUXNET sites (Fig. 5). However, the expected R_s-T_s lag across the FLUXNET sites also varies considerably, from −24.6 to 21.0 weeks. Furthermore, the R_s-T_s lag of 64% site-years is higher than ± 1 week

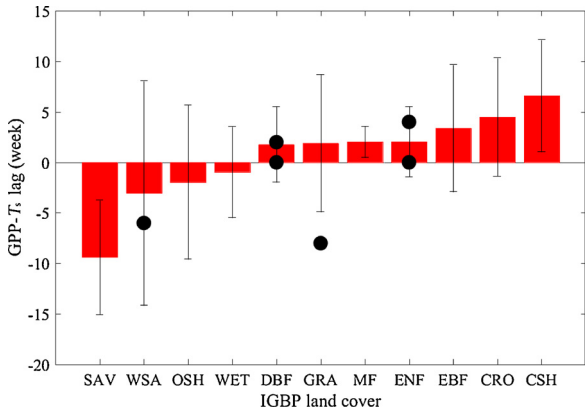

Fig. 7. Time lags between GPP and soil temperature (GPP-T_s lag) among different International Geosphere-Biosphere Programme (IGBP) vegetation types as evaluated for the FLUXNET2015 Tier1 dataset. Red bars and its error bars represent the average of the mean values and standard deviation from different sites, respectively; black points represent the lag values in the research sites selected in this study. The IGBP vegetation types are: SAV-Savannas; WSA-Woody Savannas; OSH-Open Shrublands; WET-Permanent Wetlands; DBF-Deciduous Broadleaf Forest; GRA-Grasslands; MF-Mixed Forest; ENF-Evergreen Needleleaf Forest; EBF-Evergreen Broadleaf Forest; CRO-Croplands; CSH-Closed Shrublands (For interpretation of the references to color in this figure legend, the reader is referred to the web version of this article).

(positive means T_s lags R_s, whereas negative means otherwise), implying that R_s and T_s series are generally out of phase.

4. Discussion

Hysteresis in the relationship between soil respiration and temperature suggests that important information is missing in conceptual models for R_s, including the widely used Q_{10} model (Bond-Lamberty and Thomson, 2010b; Lloyd and Taylor, 1994), which links R_s primarily to T_s. Although this phenomenon is commonly reported in the literature (see Table 1), there remains substantial disagreement on the mechanisms that determine the magnitude and direction of the hysteresis. While numerous studies have established that R_s responds exponentially to changes in T_s, recent reports of a hysteretic pattern for this relationship at seasonal timescales suggest that other factors likely mediate this relationship. Our results show that variation in GPP and θ can indeed lead to hysteresis in the R_s-T_s relationship, and that such patterns occur commonly (e.g., in nearly 60% of the site-years investigated), supporting our hypothesis. Our results provide new insights for understanding the sources of seasonal variability in R_s and demonstrate the importance of incorporating recently assimilated carbon and soil moisture into ecosystem models.

4.1. Effects of photosynthesis

Results from our modeling exercise reveal that lags in the seasonal variation of canopy photosynthesis and soil temperature can explain both clockwise and counterclockwise hysteresis patterns, depending on the direction of the lag (Fig. 1a), in a way that is consistent with field data in a wide range of sites (Fig. S3). In other words, the agreement between the model predictions and field observations supports the hypothesis that the time lag between soil respiration and temperature can originate from the lag between canopy photosynthesis and temperature (Fig. 3). Photosynthesis provides the substrate for respiration of both roots and microbes (Finzi et al., 2015; Högberg et al., 2001; Kuzyakov and Gavrichkova, 2010; Mencuccini and Hölttä, 2010; Tang et al., 2005), but belowground allocation and the transport between leaves and roots can range from hours to weeks (Baldocchi et al., 2006; Barron-Gafford et al., 2014; Kuzyakov and Cheng, 2001; Stoy et al., 2007; Tang et al., 2005; Vargas et al., 2011; Zhang et al., 2013; Zhang et al., 2015). The time lag between canopy photosynthesis and soil temperature has been previously invoked to explain the R_s-T_s hysteresis at diurnal timescales (Bahn et al., 2008; Oikawa et al., 2014; Parkin and Kaspar, 2003; Savage et al., 2013; Vargas et al., 2010; Zhang et al., 2015) and the figure-8 hysteresis pattern recorded in field experiments (Zhang et al., 2015). Our results indicate that a similar conclusion also holds at the seasonal timescale, consistent with previous work (Phillips et al., 2010). The figure-8 pattern can reflect the dynamic of substrate allocation to roots (Zhang et al., 2015), because the substrate input can significantly regulate the temperature sensitivity of soil respiration (Boone et al., 1998; Zhu and Cheng, 2011; Zhang et al., 2015). Therefore, when photosynthate supply is out of phase with T_s, simple T_s-based models will not accurately capture temporal dynamics in R_s.

Identifying the lags and hysteresis at multiple timescales between GPP and R_s across ecosystems may provide insights on the rate and timing of carbon transport from canopy to soils and back to the atmosphere (Vargas et al., 2011; Barron-Gafford et al., 2014; Zhang et al., 2015). Our analysis of the links between GPP and T_s from 129 FLUXNET sites revealed that lags between GPP and T_s were common and of significant magnitude, ranging from −25 to 25 weeks across the selected sites. The resulting R_s-T_s lag also spans a wide range from −24.6 to 21.0 weeks (Fig. 5). Negative lags between GPP and T_s (associated with counterclockwise R_s-T_s hysteresis) were more prevalent at low latitudes, whereas positive lags between GPP and T_s (associated with clockwise R_s-T_s hysteresis) were more prevalent at high latitudes (Fig. 6).

Further support for the important role of canopy photosynthesis in driving hysteresis comes from sites where plot-level experimental treatments affected the delivery of photosynthates to the soil, but did not significantly affect site micro-climate. As shown in our study, the results from US-SRM indicate that hysteresis is most pronounced in the control plots (Fig. S3g), intermediate in girdled plots (Fig. S3h), and least pronounced in the inter-canopy plots (Fig. S3i), where lower plant density probably provides lower carbon inputs to the soil. The incorporation of photosynthesis in the Q_{10} model indeed improved the model-data agreement by reproducing the R_s-T_s hysteresis for most selected sites (Fig. S6), pointing out the benefit of considering the hysteresis effect in R_s modeling, which currently still suffers from a large amount of uncertainty (Xu and Shang, 2016). To what extent these explanations hold across ecosystems still requires further exploration in the field with substrate transport measurements and time lag evaluation.

4.2. Effects of soil moisture

Our results further demonstrate that a time lag between T_s and θ can introduce the figure-8 pattern (Fig. 1b), which was observed and simulated in several field sites (see Fig. S7 and Table 3). Large lags between T_s and θ can also produce the counterclockwise hysteresis observed at US-SRM (Fig. S3g-i), which experienced significant water stress early in the growing season. Other work has demonstrated that water stress late in the growing season results in clockwise hysteresis (Gaumont-Guay et al., 2006; Harper et al., 2005; Vargas and Allen, 2008). These dynamics are linked to the fact that low θ inhibits R_s directly (e.g., Borken et al., 2006; Curiel Yuste et al., 2007; Griffis et al., 2004; Ruehr et al., 2010) either by slowing decomposition rates (Manzoni et al., 2012) or by suppressing photosynthetic rates (Chaves et al., 2002) that provide substrate for root and rhizosphere respiration. Incorporating θ effects in our simulations significantly improved the RMSE, AIC_c, and correlations between simulated and observed R_s, especially in the semi-arid sites (US-SRM and US-WKg). It should be noted that most soil biogeochemical models include both temperature and soil moisture rate modifiers for decomposition (for a review, see Bauer et al., 2008). Because of the multiplicative form of these modifiers (similar to Eqs. (3)-(2) and (7)), these models can capture

hysteretic loops driven by out-of-phase temperature and soil moisture seasonality.

4.3. Effects of substrate input

Litterfall addition has also been suggested as a possible cause of the seasonal R_s-T_s hysteresis (Curiel Yuste et al., 2005; Jassal et al., 2005; Jia et al., 2013; Oe et al., 2011). In deciduous canopies, litterfall addition late in the growing season may provide a pulse of the substrate for microbial respiration. For example, decomposition of recent litterfall contributes 12% to soil respiration in the Harvard Forest (Bowden et al., 1993). This mechanism may explain the high R_s late in the growing season at US-Ha1-E2 site in 2003, 2004 and 2006 (Figs. S3l, m and o). Intra-annual variation of decomposable substrate driven by litterfall has long been believed to decouple R_s from T_s and has been well represented in some modeling approaches (e.g., Gu et al., 2004; Kirschbaum, 2006). Similarly, plant senescence late in the growing season can also introduce clockwise hysteresis (Kirschbaum, 2004, 2006) as a result of respiration decline due to root decay (Zhang et al., 2013). In addition, the respiratory costs of fine root production can exhibit a hysteretic response to temperature (Abramoff and Finzi, 2015; Kitajima et al., 2010; but see Curiel Yuste et al., 2005), which in turn may also drive the seasonal R_s-T_s hysteresis.

Interestingly, our results reveal that the direction of hysteresis can vary in time as well as space. Within a site, the defining features of the hysteresis between R_s and T_s can change from one year to the next. For example, at US-Dk2, the direction of hysteresis changed between 2003 and 2004 (Fig. S3a and b), whereas at US-Ha1-E2, hysteresis was evident in most years, but not 2005 (Fig. S3n). Inter-annual variation in the extent to which soil respiration is substrate- or moisture-limited could explain these switches in the direction of hysteresis from one year to the next.

4.4. Hysteresis driven by autotrophic and heterotrophic respiration

The contrasting patterns in the control plots (with both heterotrophic and autotrophic respiration; Fig. S3g) and the inter-canopy plots (with heterotrophic respiration alone; Fig. S3i) at US-SRM indicate that the seasonal R_s-T_s hysteresis patterns are driven by the activity of autotrophs or heterotrophs in the soil. These results are consistent with previous studies that have more conclusively shown that heterotrophic and autotrophic respiration have different hysteresis response patterns to temperature (e.g., Savage et al., 2013; Song et al., 2015). Because autotrophic and heterotrophic respiration are controlled by different processes, thus, they may react differently to both biotic and abiotic factors (Baggs, 2006; Zhang et al., 2013). Heterotrophic respiration is primarily driven by the decomposition of soil organic carbon (either from organic matter or roots) and is therefore determined by the activity of microbes (Davidson et al., 2006a), which is in turn sensitive to both soil temperature and moisture (Manzoni et al., 2012; Moyano et al., 2013). Autotrophic respiration is driven by root metabolism, which is sensitive to photosynthetic and C allocation processes (Horwath et al., 1994), in addition to temperature (Way and Sage, 2008) and soil moisture (Chaves et al., 2002). The spatial variability of heterotrophic and autotrophic respiration may also differ. For example, Drewitt et al. (2002) reported pronounced hysteresis appearing in observations of R_s from some, but not all plots, implying a strong spatial constraint on R_s dynamics regulated by the spatial distribution of roots (Boone et al., 1998) or soil organic carbon.

4.5. Representing hysteresis in Q_{10} type models

Many efforts to predict R_s rely on a Q_{10}-type equation, where a reference respiration rate is modified by a temperature sensitivity function driven by the Q_{10} parameter. In many cases, a constant Q_{10} is commonly used to describe the temperature sensitivity of R_s, and global studies have identified convergence in Q_{10} values to ~1.4 (Bond-Lamberty and Thomson, 2010b; Mahecha et al., 2010). However, using a constant Q_{10} value has been widely challenged (e.g., Davidson et al., 2006b; Janssens and Pilegaard, 2003), as we continue to learn more about the sensitivity of Q_{10} to the depth of soil temperature measurement (Graf et al., 2008; Pavelka et al., 2007; Latimer and Risk, 2016), soil temperature range (Gaumont-Guay et al., 2006; Qi et al., 2002; Wang et al., 2014), soil moisture (Gaumont-Guay et al., 2006; Wang et al., 2014; Tucker and Reed, 2016) and C substrate supply to microbes (Davidson and Janssens, 2006). Here, we demonstrate that canopy photosynthesis and soil moisture are able to decouple R_s from T_s, leading to hysteresis. Results from this work can guide efforts to elucidate whether seasonal hysteresis in modeled soil respiration really reflects improper specification of model parameters or instead reflects the phase of key model driving variables. Our work may also be useful to further improve gap-filling strategies for ecosystem-scale carbon fluxes (e.g., Falge et al., 2001; Moffat et al., 2007) and net ecosystem exchange (NEE) partitioning methods (e.g., Reichstein et al., 2005; Stoy et al., 2006) of eddy covariance measurements, which often rely on empirical approaches to the parameterization of soil respiration models rarely reflecting its hysteresis response to temperature (Phillips et al., 2017).

4.6. Opportunities for future research

Our results, together with those from previous studies, raise a few questions for future exploration. The first concerns the extent to which the seasonal hysteresis results from the depth of soil temperature measurement (Curiel Yuste et al., 2005; Drewitt et al., 2002; Gaumont-Guay et al., 2006; Sampson et al., 2007), because the dampening of seasonal temperature fluctuations with depth (Davidson et al., 2006a; Gaumont-Guay et al., 2006) may affect the amplitude of the hysteretic loop. In addition, the seasonal hysteresis response of root phenology to temperature (Abramoff and Finzi, 2015) may provide an explanation for the observed asynchronous R_s-T_s trajectories. The numerical models presented in this study assume that soil moisture and GPP act independently on R_s. However, soil moisture may also affect respiration indirectly, via changes in GPP. Therefore, our approach cannot fully disentangle soil moisture and photosynthesis contributions to the R_s-T_s hysteresis and should motivate future work. The research sites selected in this study span a wide range of climates, but we still know little on whether the hysteresis is associated with climate. However, our synthesis of FLUXNET2015 data reveals that lags between photosynthesis and temperature vary with latitude and vegetation, thereby motivating more synthesis work on the spatial distribution of the R_s-T_s hysteresis across FLUXNET sites. Such analyses would be greatly facilitated by more standardized approaches to sharing and accessing soil respiration data in a network context like within the existing FLUXNET.

5. Conclusion

The exponential temperature response of soil respiration underlies the most commonly used soil respiration models, however, observations of soil respiration and temperature are often differentially coupled at seasonal timescales, resulting in a hysteresis effect. Because these models are so widely used in various contexts, it is important to understand the cause of these hysteretic patterns. This study applies both numerical models and data-driven analyses across AmeriFlux sites to explain the mechanisms underlying this hysteresis on a seasonal timescale. The time lag of canopy photosynthesis and soil temperature introduces a lag of soil respiration and soil temperature that explains much of the seasonal soil respiration-temperature hysteresis. The hysteresis direction depends on the direction of the time lag between canopy photosynthesis and temperature. A clockwise hysteresis appears when photosynthetic activity precedes soil temperature, and a counterclockwise hysteresis appears when photosynthetic activity lags soil

temperature. The hysteresis is suppressed when the photosynthesis effect on soil respiration is eliminated. A synthesis of FLUXNET2015 data reveals that time lags between canopy photosynthesis and temperature are sufficiently long to result in the seasonal soil respiration-temperature hysteresis, which occurs in 64% of site-years, highlighting the potential for this phenomenon to be widespread. In water-limited ecosystems, soil moisture can decouple soil respiration rate from temperature and introduce a figure-8 shaped hysteresis, and can also produce clockwise or counterclockwise hysteresis if the lag between soil temperature and soil moisture is very large, as is the case in the semi-arid ecosystems studied here. Incorporating photosynthesis or/and soil moisture in the Q_{10} model improves its explanatory power by capturing the phase of the seasonal soil respiration time series. Because of their role in modulating respiration seasonal cycles, recently assimilated carbon and soil moisture deserve special attention when dealing with the temperature response of respiration and its feedback to climate change.

Acknowledgements

The authors appreciate the constructive comments from the special issue guest editor and two anonymous reviewers. This work was supported by the AmeriFlux Management Project, administered by the US Department of Energy, and by the USDA Forest Service – Southern Research Station. Q. Zhang acknowledges support from the National Natural Science Foundation of China (Project NO. 51509187); S. Manzoni acknowledges support from the Swedish Research Councils and SIDA (VR 2016-06313 and VR 2016-04146). The authors thank E. Brzostek, C. Wayson, and T. Roman for their assistance in collecting and analyzing soil respiration data at US-MMS. The authors also appreciate the assistance from M. A. Giasson and J. W. Munger in preparing data from the US-Ha1 site. R. Scott thanks E. Hamerlynck, who was responsible for the establishment of the respiration measurements at US-SRM site. The authors thank R. Oren, T. Mandra, K. Yi, S. Denham, M. Benson, M. Medicus, and L. Young, K. Beidler, M. Craig, S. Kannenberg, A. Keller, L. Podzikowski, A. Scheibe for constructive feedback on earlier versions of the manuscript.

Appendix A. Supplementary data

Supplementary material related to this article can be found, in the online version, at doi:https://doi.org/10.1016/j.agrformet.2018.05.005.

References

Abramoff, R.Z., Finzi, A.C., 2015. Are above- and below-ground phenology in sync? New Phytol. 205 (3), 1054–1061.
Akaike, H., 1987. Factor-analysis and AIC. Psychometrika 52 (3), 317–332.
Bahn, M., Rodeghiero, M., Anderson-Dunn, M., Dore, S., Gimeno, C., Drosler, M., Williams, M., Ammann, C., Berninger, F., Flechard, C., Jones, S., Balzarolo, M., Kumar, S., Newesely, C., Priwitzer, T., Raschi, A., Siegwolf, R., Susiluoto, S., Tenhunen, J., Wohlfahrt, G., Cernusca, A., 2008. Soil respiration in European grasslands in relation to climate and assimilate supply. Ecosystems 11 (8), 1352–1367.
Baldocchi, D., Tang, J.W., Xu, L.K., 2006. How switches and lags in biophysical regulators affect spatial-temporal variation of soil respiration in an oak-grass savanna. J. Geophys. Res. Biogeo. 111, G02008. http://dx.doi.org/10.1029/2005JG000063.
Baggs, E.M., 2006. Partitioning the components of soil respiration: a research challenge. Plant Soil 284, 1–5.
Barron-Gafford, G.A., Cable, J.M., Bentley, L.P., Scott, R.L., Huxman, T.E., Jenerette, G.D., Ogle, K., 2014. Quantifying the timescales over which exogenous and endogenous conditions affect soil respiration. New Phytol. 202 (2), 442–454.
Bauer, J., Herbst, M., Huisman, J.A., Weihermuller, L., Vereecken, H., 2008. Sensitivity of simulated soil heterotrophic respiration to temperature and moisture reduction functions. Geoderma 145, 17–27.
Bond-Lamberty, B., Thomson, A., 2010a. A global database of soil respiration data. Biogeosciences 7 (6), 1915–1926.
Bond-Lamberty, B., Thomson, A., 2010b. Temperature-associated increases in the global soil respiration record. Nature 464 (7288), 579–582.
Boone, R.D., Nadelhoffer, K.J., Canary, J.D., Kaye, J.P., 1998. Roots exert a strong influence on the temperature sensitivity of soil respiration. Nature 396 (6711), 570–572.
Borken, W., Savage, K., Davidson, E.A., Trumbore, S.E., 2006. Effects of experimental drought on soil respiration and radiocarbon efflux from a temperate forest soil. Glob. Change Biol. 12 (2), 177–193.
Bowden, R.D., Nadelhoffer, K.J., Boone, R.D., Melillo, J.M., Garrison, J.B., 1993. Contributions of aboveground litter, belowground litter, and root respiration to total soil respiration in a temperature mixed hardwood Forest. Can. J. For. Res. 23 (7), 1402–1407.
Brzostek, E.R., Dragoni, D., Brown, Z.A., Phillips, R.P., 2015. Mycorrhizal type determines the magnitude and direction of root-induced changes in decomposition in a temperate forest. New Phytol. 206 (4), 1274–1282.
Burnham, K.P., Anderson, D.R., 2002. Model Selection and Multimodel Inference. A Practical Information-Theoretic Approach, second ed. Springer.
Chaves, M.M., Pereira, J.S., Maroco, J., Rodrigues, M.L., Ricardo, C.P.P., Osorio, M.L., Carvalho, I., Faria, T., Pinheiro, C., 2002. How plants cope with water stress in the field. Photosynthesis and growth. Ann. Bot. 89, 907–916.
Crill, P.M., 1991. Seasonal patterns of methane uptake and carbon dioxide release by a temperate woodland soil. Glob. Biogeochem. Cycles 5 (4), 319–334.
Curiel Yuste, J., Janssens, I.A., Ceulemans, R., 2005. Calibration and validation of an empirical approach to model soil CO_2 efflux in a deciduous forest. Biogeochemistry 73 (1), 209–230.
Curiel Yuste, J.C., Baldocchi, D.D., Gershenson, A., Goldstein, A., Misson, L., Wong, S., 2007. Microbial soil respiration and its dependency on carbon inputs, soil temperature and moisture. Glob. Change Biol. 13 (9), 2018–2035.
Davidson, E.A., Belk, E., Boone, R.D., 1998. Soil water content and temperature as independent or confounded factors controlling soil respiration in a temperate mixed hardwood forest. Glob. Change Biol. 4 (2), 217–227.
Davidson, E.A., Janssens, I.A., 2006. Temperature sensitivity of soil carbon decomposition and feedbacks to climate change. Nature 440 (7081), 165–173.
Davidson, E.A., Savage, K.E., Trumbore, S.E., Borken, W., 2006a. Vertical partitioning of CO_2 production within a temperate forest soil. Glob. Change Biol. 12 (6), 944–956.
Davidson, E.A., Janssens, I.A., Luo, Y.Q., 2006b. On the variability of respiration in terrestrial ecosystems: moving beyond Q_{10}. Glob. Change Biol. 12 (2), 154–164.
Drewitt, G.B., Black, T.A., Nesic, Z., Humphreys, E.R., Jork, E.M., Swanson, R., Ethier, G.J., Griffis, T., Morgenstern, K., 2002. Measuring forest floor CO_2 fluxes in a Douglas-fir forest. Agric. For. Meteorol. 110 (4), 299–317.
Falge, E., Baldocchi, D., Olson, R., Anthoni, P., Aubinet, M., Bernhofer, C., Burba, G., Ceulemans, R., Clement, R., Dolman, H., Granier, A., Gross, P., Grunwald, T., Hollinger, D., Jensen, N.O., Katul, G., Keronen, P., Kowalski, A., Lai, C.T., Law, B.E., Meyers, T., Moncrieff, H., Moors, E., Munger, J.W., Pilegaard, K., Rannik, U., Rebmann, C., Suyker, A., Tenhunen, J., Tu, K., Verma, S., Vesala, T., Wilson, K., Wofsy, S., 2001. Gap filling strategies for defensible annual sums of net ecosystem exchange. Agric. For. Meteorol. 107 (1), 43–69.
Finzi, A.C., Abramoff, R.Z., Spiller, K.S., Brzostek, E.R., Darby, B.A., Kramer, M.A., Phillips, R.P., 2015. Rhizosphere processes are quantitatively important components of terrestrial carbon and nutrient cycles. Glob. Change Biol. 21 (5), 2082–2094.
Gaumont-Guay, D., Black, T.A., Griffis, T.J., Barr, A.G., Jassal, R.S., Nesic, Z., 2006. Interpreting the dependence of soil respiration on soil temperature and water content in a boreal aspen stand. Agric. For. Meteorol. 140 (1-4), 220–235.
Goulden, M.L., Wofsy, S.C., Harden, J.W., Trumbore, S.E., Crill, P.M., Gower, S.T., et al., 1998. Sensitivity of boreal forest carbon balance to soil thaw. Science 279 (5348), 214–217.
Graf, A., Weihermuller, L., Huisman, J.A., Herbst, M., Bauer, J., Vereecken, H., 2008. Measurement depth effects on the apparent temperature sensitivity of soil respiration in field studies. Biogeosciences 5 (4), 1175–1188.
Griffis, T.J., Black, T.A., Gaumont-Guay, D., Drewitt, G.B., Nesic, Z., Barr, A.G., Morgenstern, K., Kljun, N., 2004. Seasonal variation and partitioning of ecosystem respiration in a southern boreal aspen forest. Agric. For. Meteorol. 125 (3-4), 207–223.
Gu, L.H., Post, W.M., King, A.W., 2004. Fast labile carbon turnover obscures sensitivity of heterotrophic respiration from soil to temperature: a model analysis. Glob. Biogeochem. Cycles 18, GB1022. http://dx.doi.org/10.1029/2003gb002119.
Harper, C.W., Blair, J.M., Fay, P.A., Knapp, A.K., Carlisle, J.D., 2005. Increased rainfall variability and reduced rainfall amount decreases soil CO_2 flux in a grassland ecosystem. Glob. Change Biol. 11 (2), 322–334.
Högberg, P., Nordgren, A., Buchmann, N., Taylor, A.F.S., Ekblad, A., Högberg, M.N., Nyberg, G., Ottosson-Löfvenius, M., Read, D.J., 2001. Large-scale forest girdling shows that current photosynthesis drives soil respiration. Nature 411, 789–792.
Horwath, W.R., Pregitzer, K.S., Paul, E.A., 1994. 14C allocation in tree-soil systems. Tree Physiol. 14, 1163–1176.
Irvine, J., Law, B.E., 2002. Contrasting soil respiration in young and old-growth ponderosa pine forests. Glob. Change Biol. 8 (12), 1183–1194.
Janssens, I.A., Pilegaard, K., 2003. Large seasonal changes in Q_{10} of soil respiration in a beech forest. Glob. Change Biol. 9 (6), 911–918.
Jassal, R., Black, A., Novak, M., Morgenstern, K., Nesic, Z., Gaumont-Guay, D., 2005. Relationship between soil CO_2 concentrations and forest-floor CO_2 effluxes. Agric. For. Meteorol. 130 (3-4), 176–192.
Jia, X., Zha, T.S., Wu, B., Zhang, Y.Q., Chen, W.J., Wang, X.P., Yu, H.Q., He, G.M., 2013. Temperature response of soil respiration in a Chinese pine plantation: hysteresis and seasonal vs. diel Q_{10}. PloS One 8, E57858. http://dx.doi.org/10.1371/journal.pone.0057858.
Kirschbaum, M.U.F., 2004. Soil respiration under prolonged soil warming: are rate reductions caused by acclimation or substrate loss? Glob. Change Biol. 10 (11), 1870–1877.
Kirschbaum, M.U.F., 2006. The temperature dependence of organic-matter

decomposition - still a topic of debate. Soil Biol. Biochem. 38 (9), 2510–2518.
Kitajima, K., Anderson, K.E., Allen, M.F., 2010. Effect of soil temperature and soil water content on fine root turnover rate in a California mixed conifer ecosystem. J. Geophys. Res. 115, G04032. http://dx.doi.org/10.1029/2009JG001210.
Knapp, A.K., Conard, S.L., Blair, J.M., 1998. Determinants of soil CO_2 flux from a sub-humid grassland: effect of fire and fire history. Ecol. Appl. 8 (3), 760–770.
Kominami, Y., Jomura, M., Ataka, M., Miyama, T., Dannoura, M., Makita, et al., 2012. Heterotrophic respiration causes seasonal hysteresis in soil respiration in a warm-temperate forest. J. For. Res. 17 (3), 296–304.
Kuzyakov, Y., Cheng, W., 2001. Photosynthesis controls of rhizosphere respiration and organic matter decomposition. Soil Biol. Biochem. 33 (14), 1915–1925.
Kuzyakov, Y., Gavrichkova, O., 2010. Review: time lag between photosynthesis and carbon dioxide efflux from soil: a review of mechanisms and controls. Glob. Change Biol. 16 (12), 3386–3406.
Latimer, R.N.C., Risk, D.A., 2016. An inversion approach for determining distribution of production and temperature sensitivity of soil respiration. Biogeosciences 13 (7), 2111–2122.
Lloyd, J., Taylor, J.A., 1994. On the temperature-dependence of soil respiration. Funct. Ecol. 8 (3), 315–323.
Luo, Y.Q., Wan, S.Q., Hui, D.F., Wallace, L.L., 2001. Acclimatization of soil respiration to warming in a tall grass prairie. Nature 413 (6856), 622–625.
Mahecha, M.D., Reichstein, M., Carvalhais, N., Lasslop, G., Lange, H., Seneviratne, S.I., Vargas, R., Ammann, C., Arain, M.A., Cescatti, A., Janssens, I.A., Migliavacca, M., Montagnani, L., Richardson, A.D., 2010. Global convergence in the temperature sensitivity of respiration at ecosystem level. Science 329 (5993), 838–840.
Manzoni, S., Schimel, J.P., Porporato, A., 2012. Responses of soil microbial communities to water stress: results from a meta-analysis. Ecology 93 (4), 930–938.
Morén, A.S., Lindroth, A., 2000. CO_2 exchange at the floor of a boreal forest. Agric. For. Meteorol. 101 (1), 1–14.
Moyano, F.E., Manzoni, S., Chenu, C., 2013. Responses of soil heterotrophic respiration to moisture availability: an exploration of processes and models. Soil Biol. Biochem. 59, 72–85.
Mencuccini, M., Hölttä, T., 2010. The significance of phloem transport for the speed with which canopy photosynthesis and belowground respiration are linked. New Phytol. 185 (1), 189–203.
Moffat, A.M., Papale, D., Reichstein, M., Hollinger, D.Y., Richardson, A.D., Barr, A.G., Beckstein, C., Braswell, B.H., Churkina, G., Desai, A.R., Falge, E., Gove, J.H., Heimann, M., Hui, D.F., Jarvis, A.J., Kattge, J., Noormets, A., Stauch, V.J., 2007. Comprehensive comparison of gap-filling techniques for eddy covariance net carbon fluxes. Agric. For. Meteorol. 147 (3-4), 209–232.
Munger, W., Wofsy, S., 1999. Canopy-Atmosphere Exchange of carbon, water and energy at harvard Forest EMS Tower since 1991. Harvard Forest Data Archive: HF004.
Novick, K.A., Oishi, A.C., Ward, E.J., Siqueira, M., Juang, J.Y., Stoy, P.C., 2015. On the difference in the net ecosystem exchange of CO_2 between deciduous and evergreen forests in the southeastern United States. Glob. Change Biol. 21 (2), 827–842.
Novick, K.A., Oren, R., Stoy, P.C., Siqueira, M.B.S., Katul, G.G., 2009. Nocturnal evapotranspiration in eddy-covariance records from three co-located ecosystems in the southeastern US: implications for annual fluxes. Agric. For. Meteorol. 149 (9), 1491–1504.
Oe, Y., Yamamoto, A., Mariko, S., 2011. Characteristics of soil respiration temperature sensitivity in a Pinus/Betula mixed forest during periods of rising and falling temperatures under the Japanese monsoon climate. J. Ecol. Field Biol. 34, 193–202.
Oikawa, P.Y., Grantz, D.A., Chatterjee, A., Eberwein, J.E., Allsman, L.A., Jenerette, G.D., 2014. Unifying soil respiration pulses, inhibition, and temperature hysteresis through dynamics of labile soil carbon and O_2. J. Geophys. Res. Biogeo. 119 (4), 521–536.
Oishi, A.C., Palmroth, S., Butnor, J.R., Johnsen, K.H., Oren, R., 2013. Spatial and temporal variability of soil CO_2 efflux in three proximate temperate forest ecosystems. Agric. For. Meteorol. 171, 256–269.
Parkin, T.B., Kaspar, T.C., 2003. Temperature controls on diurnal carbon dioxide flux: implications for estimating soil carbon loss. Soil Sci. Soc. Am. J. 67 (6), 1763–1772.
Pavelka, M., Acosta, M., Marek, M.V., Kutsch, W., Janous, D., 2007. Dependence of the Q_{10} values on the depth of the soil temperature measuring point. Plant Soil 292 (1-2), 171–179.
Phillips, C.L., Bond-Lamberty, B., Desai, A.R., Lavoie, M., Risk, D., Tang, J., Todd-Brown, K., Vargas, R., 2017. The value of soil respiration measurements for interpreting and modeling terrestrial carbon cycling. Plant Soil 413 (1-2), 1–25.
Phillips, C.L., Nickerson, N., Risk, D., Bond, B.J., 2011. Interpreting diel hysteresis between soil respiration and temperature. Glob. Change Biol. 17 (1), 515–527.
Phillips, S.C., Varner, R.K., Frolking, S., Munger, J.W., Bubier, J.L., Wofsy, S.C., Crill, P.M., 2010. Interannual, seasonal, and diel variation in soil respiration relative to ecosystem respiration at a wetland to upland slope at Harvard forest. J. Geophys. Res. Biogeo. 115, G02019. http://dx.doi.org/10.1029/2008jg000858.
Qi, Y., Xu, M., Wu, J.G., 2002. Temperature sensitivity of soil respiration and its effects on ecosystem carbon budget: nonlinearity begets surprises. Ecol. Model. 153 (1-2), 131–142.
Raich, J.W., Schlesinger, W.H., 1992. The global carbon-dioxide flux in soil respiration and its relationship to vegetation and climate. Tellus B 44 (2), 81–99.
Reichstein, M., Falge, E., Baldocchi, D., Papale, D., Aubinet, M., Berbigier, P., Bernhofer, C., Buchmann, N., Gilmanov, T., Granier, A., Grunwald, T., Havrankova, K., Ilvesniemi, H., Janous, D., Knohl, A., Laurila, T., Lohila, A., Loustau, D., Matteucci, G., Meyers, T., Miglietta, F., Ourcival, J.M., Pumpanen, J., Rambal, S., Rotenberg, E., Sanz, M., Tenhunen, J., Seufert, G., Vaccari, F., Vesala, T., Yakir, D., Valentini, R., 2005. On the separation of net ecosystem exchange into assimilation and ecosystem respiration: review and improved algorithm. Glob. Change Biol. 11 (9), 1424–1439.
Ruehr, N.K., Knohl, A., Buchmann, N., 2010. Environmental variables controlling soil respiration on diurnal, seasonal and annual time-scales in a mixed mountain forest in Switzerland. Biogeochemistry 98 (1-3), 153–170.
Sampson, D.A., Janssens, I.A., Curiel Yuste, J., Ceulemans, R., 2007. Basal rates of soil respiration are correlated with photosynthesis in a mixed temperate forest. Glob. Change Biol. 13 (9), 2008–2017.
Savage, K., Davidson, E.A., Richardson, A.D., 2008. A conceptual and practical approach to data quality and analysis procedures for high-frequency soil respiration measurements. Funct. Ecol. 22, 1000–1007.
Savage, K., Davidson, E.A., Tang, J., 2013. Diel patterns of autotrophic and heterotrophic respiration among phenological stages. Glob. Change Biol. 19 (4), 1151–1159.
Schmid, H.P., Grimmond, C.S.B., Cropley, F., Offerle, B., Su, H.B., 2000. Measurements of CO_2 and energy fluxes over a mixed hardwood forest in the mid-western United States. Agric. For. Meteorol. 103 (4), 357–374.
Scott, R.L., Biederman, J.A., Hamerlynck, E.P., Barron-Gafford, G.A., 2015. The carbon balance pivot point of southwestern U.S. semiarid ecosystems: insights from the 21st century drought. J. Geophys. Res. Biogeo. 120, 2612–2624. http://dx.doi.org/10.1002/2015JG003181.
Song, W., Chen, S., Zhou, Y., Wu, B., Zhu, Y., Lu, Q., Lin, G., 2015. Contrasting diel hysteresis between soil autotrophic and heterotrophic respiration in a desert ecosystem under different rainfall scenarios. Sci. Rep. 5. http://dx.doi.org/10.1038/srep16779.
Stoy, P.C., Katul, G.G., Siqueira, M.B.S., Juang, J.Y., Novick, K.A., Uebelherr, J.M., Oren, R., 2006. An evaluation of models for partitioning eddy covariance-measured net ecosystem exchange into photosynthesis and respiration. Agric. For. Meteorol. 141 (1), 2–18.
Stoy, P.C., Palmroth, S., Oishi, A.C., Siqueira, M.B.S., Juang, J.Y., Novick, K.A., Ward, E.J., Katul, G.G., Oren, R., 2007. Are ecosystem carbon inputs and outputs coupled at short time scales? A case study from adjacent pine and hardwood forests using impulse-response analysis. Plant Cell Environ. 30 (6), 700–710.
Sulman, B.N., Roman, D.T., Scanlon, T.M., Wang, L., Novick, K.A., 2016. Comparing methods for partitioning a decade of carbon dioxide and water vapor fluxes in a temperate forest. Agric. For. Meteorol. 226, 229–245.
Suseela, V., Conant, R.T., Wallenstein, M.D., Dukes, J.S., 2012. Effects of soil moisture on the temperature sensitivity of heterotrophic respiration vary seasonally in an old-field climate change experiment. Glob. Change Biol. 18 (1), 336–348.
Tang, J.W., Baldocchi, D.D., Xu, L., 2005. Tree photosynthesis modulates soil respiration on a diurnal time scale. Glob. Change Biol. 11 (8), 1298–1304.
Tucker, C.L., Reed, S.C., 2016. Low soil moisture during hot periods drives apparent negative temperature sensitivity of soil respiration in a dryland ecosystem: a multi-model comparison. Biogeochemistry 128 (1-2), 155–169.
Van Gorsel, E., Delpierre, N., Leuning, R., Black, A., Munger, J.W., Wofsy, S., et al., 2009. Estimating nocturnal ecosystem respiration from the vertical turbulent flux and change in storage of CO_2. Agric. For. Meteorol. 149 (11), 1919–1930.
Vargas, R., Allen, M.F., 2008. Environmental controls and the influence of vegetation type, fine roots and rhizomorphs on diel and seasonal variation in soil respiration. New Phytol. 179 (2), 460–471.
Vargas, R., Baldocchi, D.D., Allen, M.F., Bahn, M., Black, T.A., Collins, S.L., Yuste, J.C., Hirano, T., Jassal, R.S., Pumpanen, J., Tang, J.W., 2010. Looking deeper into the soil: biophysical controls and seasonal lags of soil CO_2 production and efflux. Ecol. Appl. 20 (6), 1569–1582.
Vargas, R., Baldocchi, D.D., Bahn, M., et al., 2011. On the multi-temporal correlation between photosynthesis and soil CO_2 efflux: reconciling lags and observations. New Phytol. 191, 1006–1017.
Verburg, P.S.J., Larsen, J., Johnson, D.W., Schorran, D.E., Arnone, J.A., 2005. Impacts of an anomalously warm year on soil CO_2 efflux in experimentally manipulated tallgrass prairie ecosystems. Glob. Change Biol. 11 (10), 1720–1732.
Wang, B., Zha, T.S., Jia, X., Wu, B., Zhang, Y.Q., Qin, S.G., 2014. Soil moisture modifies the response of soil respiration to temperature in a desert shrub ecosystem. Biogeosciences 11 (2), 259–268.
Way, D.A., Sage, R.F., 2008. Thermal acclimation of photosynthesis in black spruce [Picea mariana (Mill.) BSP]. Plant Cell Environ. 31 (9), 1250–1262.
Xu, M., Shang, H., 2016. Contribution of soil respiration to the global carbon equation. J. Plant Physiol. 203, 16–28.
Zhang, Q., Katul, G.G., Oren, R., Daly, E., Manzoni, S., Yang, D.W., 2015. The hysteresis response of soil CO_2 concentration and soil respiration to soil temperature. J. Geophys. Res. Biogeo. 120 (8), 1605–1618.
Zhang, Q., Lei, H.M., Yang, D.W., 2013. Seasonal variations in soil respiration, heterotrophic respiration and autotrophic respiration of a wheat and maize rotation cropland in the North China plain. Agric. For. Meteorol. 180, 34–43.
Zhang, Q., Manzoni, S., Katul, G., Porporato, A., Yang, D.W., 2014. The hysteretic evapotranspiration- vapor pressure deficit relation. J. Geophys. Res. Biogeo. 119 (2), 125–140.
Zhu, B., Cheng, W., 2011. Rhizosphere priming effect increases the temperature sensitivity of soil organic matter decomposition. Glob. Change Biol. 17 (6), 2172–2183.